



HAL
open science

Effect of the loading frequency on the sand liquefaction behaviour in cyclic triaxial tests

Zhehao Zhu, Feng Zhang, Qingyun Peng, Jean Claude Dupla, Jean Canou, Gwendal Cumunel, Evelyne Foerster

► **To cite this version:**

Zhehao Zhu, Feng Zhang, Qingyun Peng, Jean Claude Dupla, Jean Canou, et al.. Effect of the loading frequency on the sand liquefaction behaviour in cyclic triaxial tests. *Soil Dynamics and Earthquake Engineering*, 2021, 147, pp.106779. 10.1016/j.soildyn.2021.106779 . hal-04313255

HAL Id: hal-04313255

<https://hal.science/hal-04313255v1>

Submitted on 22 Jul 2024

HAL is a multi-disciplinary open access archive for the deposit and dissemination of scientific research documents, whether they are published or not. The documents may come from teaching and research institutions in France or abroad, or from public or private research centers.

L'archive ouverte pluridisciplinaire **HAL**, est destinée au dépôt et à la diffusion de documents scientifiques de niveau recherche, publiés ou non, émanant des établissements d'enseignement et de recherche français ou étrangers, des laboratoires publics ou privés.



Distributed under a Creative Commons Attribution - NonCommercial 4.0 International License

1 **Effect of the loading frequency on the sand liquefaction**
2 **behaviour in cyclic triaxial tests**
3

4 **Zhehao Zhu^{a,b}, Feng Zhang^{a,*}, Qingyun Peng^a, Jean-Claude Dupla^a, Jean Canou^a, Gwendal**
5 **Cumunel^a, Evelyne Foerster^b**

6
7 ^aEcole des Ponts ParisTech, Laboratoire Navier, 6-8 av. Blaise Pascal, 77455 Marne La Vallée
8 cedex 2, France

9
10 ^bCommissariat à l'énergie Atomique, DEN, DANS, DM2S, Université Paris-Saclay, F-91191
11 Gif-sur-Yvette, France

12
13
14
15
16 ***Corresponding Author:**

17 Feng Zhang

18 Ecole des Ponts ParisTech

19 Laboratoire Navier, 6-8 av. Blaise Pascal, 77455 Marne La Vallée cedex 2, France

20 Email: feng.zhang@enpc.fr

27 Abstract

28 This study was aimed at highlighting the effect of loading frequency on the sand liquefaction
29 response by performing cyclic triaxial tests in both stress-controlled and strain-controlled modes.
30 For the first case, dense ($I_{Dmat}=0.70$) and medium-dense ($I_{Dmat}=0.55$) sand specimens were
31 subjected to alternative and non-alternative axial stresses; whilst dense ($I_{Dmat}=0.70$) sand
32 specimens were subjected to alternative axial strain over a wide range of loading frequencies in
33 the second case. It was experimentally found that in the case of alternative loading for test
34 specimens with $I_{Dmat}=0.70$ in stress-controlled mode, the effect of the loading frequency was not
35 notable for dry sand specimens. In contrast, the effect of the loading frequency was significant
36 for saturated sand specimens in both the loading modes. This was because, upon shearing,
37 transient deformation occurred with the presence of excess pore water pressure, during which the
38 inertia force needed to be taken into account. In the axial direction, the inertia force opposing the
39 external loading certainly increased the liquefaction resistance by suppressing the complete
40 development of the sand liquefaction. As for non-alternative loading in stress-controlled mode
41 for test specimens with $I_{Dmat}=0.55$, the loading frequency played a vital role in pure extensional
42 loading, which could also be logically attributed to the presence of the axial inertia force
43 appearing in the large strain and transient deformation stages. However, the effect of the loading
44 frequency on the compressive pattern was unclear due to the following two reasons: (i) the
45 inertia force in the lateral direction appeared in the form of enhancing lateral confinement,
46 thereby impeding the relative sliding; and (ii) during shearing, the rearrangement of the sand
47 grains occurred in a more stable direction. These two aspects both provided beneficial
48 contribution to sand liquefaction resistance, thereby preventing the occurrence of transient
49 deformation. Under the circumstance, the sand specimens deformed only moderately, thereby
50 eliminating the need to consider the role of the loading frequency.

51

52 Keywords: Sand liquefaction; Loading frequency; Cyclic triaxial tests; Alternative and non-
53 alternative loadings

54

55 1. Introduction

56 Sand liquefaction has emerged as an engaging topic in geotechnical engineering since the
57 occurrence of the Niigata earthquake in Japan [1] and Alaska earthquake in the United States [2].
58 Under seismic loading, liquefaction may result in catastrophic consequences (e.g., transient
59 deformation) pertaining to above-ground structures and underground lifelines due to the rapid
60 build-up of excess pore water pressure [3]. According to the “Seed-equivalent method” [4]
61 that simplifies the recorded irregular earthquake shear stresses to an alternative equal-amplitude
62 loading, the liquefaction potential has been commonly assessed by performing cyclic triaxial
63 tests in laboratory research. Due to the inherent limitation of actuator devices, experimental work
64 has been mostly conducted under a lower level of loading frequencies, for instance 0.05 Hz [5],
65 0.10 Hz [6–8], 0.20 Hz [9], 1 Hz [10,11] and etc., in order to better control the imposed loading,
66 as well as overcome the measurement problems of the rapid excess pore water pressure and axial
67 strain. However, the frequency of a real seismic excitation typically varies in the range of a few
68 hertz [12–14], which indicates the effect of this element is also a pronounced parameter that
69 needs to be underlined in laboratory tests [15].

70 Considerable research has been devoted to examine this aspect over the past fifty years.
71 However, no clear consensus has been accomplished, and diverse views still exist in the
72 published literature as to whether the commonly used lower frequency values are conservative or
73 radical in the context of earthquake engineering. In general, the outcomes of earlier
74 investigations revealed an ignorable effect of loading frequency [16–20] on the liquefaction
75 response. For instance, a Roscoe-type simple shear device was applied by Peacock [16] to
76 examine the liquefaction potential of medium-dense saturated Monterey sand under different
77 loading frequencies within the range of 0.17-4 Hz. However, no clear tendency of the loading
78 frequency was observed since the obtained experimental data dispersed within $\pm 10\%$ of the
79 mean value. Similar results have also been reported by other investigators, including Yoshimi
80 [17] and Tatsuoka [18,19], who performed ring torsion and cyclic triaxial tests on medium-dense
81 Bandaijima and Toyoura sands, respectively. More recently, certain conclusions have been
82 repeatedly derived, albeit in a seemingly at least controversial manner. For instance, a series of
83 cyclic simple shear tests was carried out by Nong [21] on loose and dense specimens (density
84 index $I_d= 0.40$ and 0.80 , respectively) by varying the loading frequency from 0.05 to 1 Hz. The

85 experimental results showed that (i) the number of cycles to attain a given failure criterion
86 increased with the loading frequency; and (ii) the accumulated excess pore water pressure
87 decreased with the loading frequency. These two phenomena indicated a lower liquefaction
88 potential under a higher loading frequency, which is in agreement with the other reports [22–26].
89 In contrast to this beneficial contribution of loading frequency to liquefaction resistance, Mulilis
90 [27] seemed to be the first to observe a totally reversed trend that the sand specimen examined at
91 a frequency of 0.017 Hz was approximately 20% more resistant than that at a frequency of 1 Hz.
92 Similarly, Dash [28] demonstrated the enhancement of the cyclic resistance of original
93 Ahmadabad sand with a decrease in the loading frequency.

94 Table 1 summarizes the references mentioned above and it can be noted that the
95 divergence in the effect of the loading frequency seems not to be possibly attributed to the
96 employed test method, density of the sand specimen or failure criteria to identify the initial
97 liquefaction. Furthermore, in these studies, the majority of attentions were paid to assessing the
98 alternative loading pattern, owing to which, the eventual mechanism in pure extensional and
99 compressive cycles could not be completely addressed. **For this purpose, the emphasis of this
100 study was put on (i) performing stress-controlled cyclic triaxial tests on saturated sand specimens
101 subjected to both alternative and non-alternative loadings in order to separate the possible
102 responses in the extensional/compressive cycles from the integrated alternative ones; and (ii)
103 performing strain-controlled cyclic triaxial tests over a sizable frequencies range (up to 5 Hz) in
104 order to directly underline the dynamic deformation characteristics. In addition, dry sand
105 specimens were also adopted in stress-controlled triaxial programme to clarify the sliding
106 mechanism of the sand grains without the interaction of the pore water under different loading
107 frequencies.**

108

109 2. Material and methods

110 2.1. Physical properties of the test material

111 The sand used in this study is a poorly graded Hostun 31 sand (termed “HN31” hereafter),
112 which is characterized by uniform sub-angular grains [6,29] and widely used in many
113 laboratories in Europe. The grain size distribution curve of HN31 sand [29] determined through
114 the laser diffraction method [30] is depicted in Figure 1. The principle of this method is that
115 while passing through a laser beam, a particle could scatter the light at a certain angle and
116 intensity linking to its grain size. The detailed index properties are listed in Table 2.

117

118 2.2. Cyclic triaxial test apparatus

119 One of the most important features required of the cyclic triaxial device for sand liquefaction
120 analysis is that the vertical piston must be firmly connected to the upper triaxial base so as to
121 generate two-way alternative loading, in which cyclic stress could reverse its direction from
122 triaxial compression to extension and vice versa. In this work, an advanced cyclic triaxial device
123 (Mono50kN [7,31]) developed in the Navier laboratory of Ecole des Ponts ParisTech was
124 employed. The vertical actuator of Mono50kN is connected to a PID (Proportional-Integral-
125 Derivative) controller. In stress-controlled mode, the test specimen could be further subjected to
126 equal-amplitude alternative shearing on its 45° plane after attaining the isotropic consolidation
127 state of $K_c=1$ (consolidation stress ratio, $K_c=\sigma'_a/\sigma'_r$) as that generated on the horizontal plane
128 [32] on the ground during earthquakes. This is the basis on which the cyclic triaxial test is
129 warranted as a meaningful approach to assess the sand liquefaction behaviour [33]. Near the final
130 part of the test, the employed PID controller probably fails since total material softening occurs
131 with sand liquefaction; accordingly, the applied loading frequency should be limited to a lower
132 range. In strain-controlled mode, the test specimen is subjected to equal-amplitude cyclic axial
133 strain in each loading cycle; as a result, the axial displacement of test specimen is exactly the
134 same as the given imposed loading. In addition, very high loading frequency is achievable in this
135 mode since the axial displacement is prescribed and irrespective of sand liquefaction softening.

136

137 2.3. Cyclic test programme

138 The test programme is summarized in Table 3. For stress-controlled tests, it should be mentioned
139 that (i) in order to ensure a suitable scale for the number of cycles to well distinguish any
140 possible behaviour from various deformation ranges, dense sand specimens with a density index
141 of sand matrix $I_{Dmat}=0.70$ were sheared in a moderate alternative pattern of $T_{cc}=0.22$ (cyclic
142 stress ratio $T_{cc}=\tau/\sigma'_c=\sigma'_d/2\sigma'_c$, where τ , σ'_c and σ'_d denote the shear, effective confining and
143 imposed deviator stresses, respectively) in CTT1-7; and (ii) considering the fact that sand
144 specimens normally become more resistant when subjected to non-alternative loading [6], as
145 verified in the preliminary tests conducted in this work, high-level non-alternative extensional
146 (CTT8-10) and compressive (CTT11-13) loading patterns with $T_{cc}=0.60$ were thus implemented
147 on medium-dense sand specimens with $I_{Dmat}=0.55$ so as to (i) control the test duration to be in an
148 acceptable range; and (ii) eliminate the need to consider any possible leakage of the fragile latex
149 membrane in the long term. For strain-controlled tests, all test specimens (CTT14-18) underwent
150 an imposed alternative strain in the axial direction with a peak value of $\varepsilon_a=\pm 0.40\%$ and a very
151 high loading frequency of $f=5.00$ Hz was included in the test programme for a better viewing of
152 pure dynamic deformation characteristic, as explained previously.

153 The cylindrical specimen with a diameter and height of 100 mm and 200 mm,
154 respectively, was fabricated with 10 layers and each layer was carefully introduced into a split
155 mould followed by slight compaction efforts (e.g., dry tamping method [34]) to achieve the
156 required thickness (20 mm) by using a hand-held tamper. Once the test specimen was generated,
157 the top triaxial base was mounted and sealed with a water-tight O-ring. Subsequently, a slight
158 vacuum of approximately 20 kPa was applied to minimize any possible disturbances while
159 removing the split mould, as well as to check the leakage of the latex membrane. Before
160 initiating the three-step saturation for the saturated specimen (e.g., CTT4-18), the confining
161 pressure was increased to 100 kPa to maintain the test specimen. Carbon dioxide (CO₂) was
162 firstly purged into the dry specimen to evacuate the air bubbles, followed by the injection of de-
163 aired water to saturate the test specimen. Note that the flux of both the CO₂ and de-aired was
164 minimized to avoid disturbing the soil fabric. Thirdly, in order to render the test specimen fully
165 saturated, the back and confining pressures were alternatively increased in small steps of
166 approximately 20 kPa until Skempton's B value ($B=\Delta u/\Delta\sigma_{con}$, where Δu and $\Delta\sigma_{con}$ denote the

167 variation in the excess water pressure and imposed confining pressure, respectively) was equal to
168 or greater than 0.98, which is believed to be high enough for the saturation of sandy soil. As for
169 dry sand specimens (e.g., CTT1-3), the confining pressure was also increased to 100 kPa without
170 performing the aforementioned saturation step.

171

172 3. Experimental results

173 3.1. Repeatability test

174 Figure 2a and Figure 2b illustrate the evolutions of the deviator stress q with the axial strain ε_a
175 and those of the excess pore water pressure Δu with the number of cycles N_{cyc} , respectively, with
176 the two parallel specimens having identical test parameters (e.g., CTT6 in stress-controlled
177 mode). It appears from Figure 2a that two stress-strain curves nearly coincided with each other;
178 from Figure 2b that (i) before r_u (excess pore water pressure ratio, $r_u = \Delta u / \sigma'_c$) attaining a
179 relatively high level of approximately 0.80, two curves were almost the same; (ii) beyond this
180 point, certain differences were observed (e.g., $r_u > 0.80$) owing to the fact that the vertical
181 hydraulic actuator could not, at this stage, manage the transient variation of the axial
182 displacement when the test specimen approached the liquefaction stage with a high accumulated
183 value of Δu . Therefore, these two phenomena suggest that the test programme adopted in this
184 study was deemed to be adequate with respect to the repeatability requirements.

185

186 3.2. Stress-controlled mode

187 3.2.1. Dry sand specimens subjected to alternative loading

188 Figure 3a shows the relationship between the axial strain ε_a and number of cycles N_{cyc} of the dry
189 sand specimens (CTT1-3) subjected to alternative shearing of T_{cc} equal to 0.22 under distinct
190 loading frequencies f of 0.02, 0.10 and 0.60 Hz. Although the minimum and maximum ε_a of dry
191 sand specimens were quite small and of the order of approximately 10^{-3} , the corresponding
192 amplitude of shear strain ($\gamma = (1 + \nu)\varepsilon_a$, where ν denotes the Poisson's ratio) were still in excess of
193 the threshold value of shear strain γ_{th} (typically around 10^{-4} [33]) on behalf of the initiation of the
194 cyclic degradation in the elasto-plastic regime. Despite the fact that the loading frequency f was
195 significantly increased by 30 times (from $f = 0.02$ to 0.60 Hz), only a minor variation was
196 recorded. This insignificant effect upon the loading frequency could not be possibly ascribed to
197 the pure elastic behaviour of the dry sand specimen since plasticity (e.g., irreversible relative
198 sliding of the sand grains) certainly occurred as explained previously ($\varepsilon_a > \gamma_{th}$).

199 Figure 3b presents the corresponding effective stress paths of the dry sand specimens.
200 The three curves appeared to be nearly identical, reconfirming that the applied loading frequency

201 exerted a negligible effect on the dry sand specimens. It is interesting to note that although the
202 drainage lines were definitively closed during shearing, the effective stress paths tended to
203 follow a straight line with a slope of 3:1 (similar to those observed in triaxial drained tests),
204 which indicated that neither excess pore water pressure nor excess air pressure occurred **during**
205 **shearing**.

206

207 3.2.2. Saturated sand specimens subjected to alternative loading

208 The experimental results of saturated sand subjected to alternative shearing of T_{cc} equal to
209 0.22 under distinct loading frequencies f of 0.02, 0.10, 0.30 and 0.60 Hz (**CTT4-7**) are regrouped
210 in the subplots of Figure 4. The imposed deviator stress σ_a acting on the test specimens sketched
211 in Figure 4a suggests that prior to the triggering of the liquefaction response, the vertical
212 hydraulic actuator remained able to generate the desired loading with a high robustness in the
213 target range of loading frequencies (from $f=0.02$ to 0.60 Hz). The relationship between Δu and
214 N_{cyc} depicted in Figure 4b shows that (i) the so-called “M line” [7,35,36] became increasingly
215 notable while approaching $r_u=1$, indicating the occurrence of cyclic **mobility** of the dense sand
216 specimen [6,7]; (ii) the applied loading frequencies played a vital role on the saturated sand
217 response, compared with the dry sand specimens; and (iii) for a given number of cycles, Δu
218 significantly increased as the loading frequency decreased. The relationship between ε_a and N_{cyc}
219 depicted in Figure 4c suggests that (i) the observed strain range of the saturated specimens was
220 dramatically larger than that of the dry sand specimens; (ii) in the initial phase of loading (e.g.,
221 $N_{cyc} \leq 10$), ε_a did not exhibit considerable fluctuations with the variation in the loading frequency;
222 (iii) nevertheless, this difference became increasingly conspicuous with further loading after
223 triggering transient deformation near the liquefaction stage; (iv) the number of cycles
224 corresponding to the attainment of the considered failure criterion (e.g., $\varepsilon_a=-3\%$ in the single
225 amplitude case) decreased with the decrease in the loading frequency. Note that the conventional
226 failure criterion of $\varepsilon_a=5\%$ in the double amplitude case (or “peak-to-peak”) **for stress-**
227 **controlled tests** [33] was not employed in the present work since at a higher loading frequency,
228 the generation of the desired loading pattern became extremely difficult, especially after the
229 triggering of the liquefaction softening, particularly for $f=0.60$ Hz. Therefore, the failure criterion

230 of $\varepsilon_a = -3\%$ in the single amplitude was specially set as an alternative, allowing the test specimen
231 to be evaluated with a higher level of confidence.

232 3.2.3. Saturated sand specimens subjected to non-alternative loading

233 Figure 5a describes the relationship between q and ε_a in the case of saturated sand subjected to
234 non-alternative extensional loading (CTT8-10). Two different responses were observed: (i) in the
235 initial loading phase, the three curves nearly coincided with one another; (ii) when subjected to
236 further shearing, the test specimen deformed increasingly quickly and a notable dispersion was
237 observed among the three curves while approaching the transient deformation stage. Figure 5b
238 shows the corresponding evolution of Δu with respect to N_{cyc} and it can be seen that the Δu was
239 initially positive due to the unloading volume-contraction effect (outlined through the purple
240 circle) upon shearing. The same phenomenon has been previously reported and attributed to the
241 reversible dilatancy by Li [37,38]. With further extensional loading, Δu steadily increased as
242 cyclic axial stress was applied, and the specimen with lower $f = 0.02$ Hz (marked in blue) tended
243 to exhibit a slightly higher absolute value of Δu in both the phases (loading and releasing, as
244 shown in Figure 5b) until the failure than that pertaining to the specimens with $f = 0.10$ Hz
245 (marked in red) and $f = 0.30$ Hz (marked in green).

246 Figure 6a presents the relationship between q and ε_a in the case of saturated sand
247 subjected to non-alternative compressive loading (CTT11-13). No clear impact of the loading
248 frequency was observed. It is worth noting that as compared with that in non-alternative
249 extensional loading, ε_a developed in a non-alternative compressive pattern under three distinct
250 loading frequencies was deemed to be in a small range. Figure 6b shows the corresponding Δu in
251 terms of N_{cyc} , and it can be seen that after the initial rapid increase, all the Δu were converged to
252 approximately $r_u = 0.60$ and the effect of the loading frequency could be considered to be trivial.

253 Figure 7 synthesizes the accumulated axial strain ε_a with respect to N_{cyc} under extensional
254 (case a) and compressive (case b) loadings. In the first six loading cycles (as shown in Figure 7)
255 in case a, no remarkable dispersion in ε_a was observed with the three loading frequencies.
256 However, the strain rate continually (e.g., $N_{cyc} > 6$) accelerated afterward, and the transient
257 deformation was finally triggered. At this stage, the applied loading frequencies played a
258 dominant role, indicating that a higher loading frequency (e.g., $f = 0.30$ Hz) seemed to be able to

259 suppress the further development of ε_a . In case b, ε_a varied in a more moderate manner in all the
260 loading ranges and finally stabilized to a certain level. In terms of the effect of the applied
261 loading frequencies, only a minor variation was recorded, in contrast to that in case a.

262 3.3. Strain-controlled mode

263 3.3.1. Saturated sand specimens subjected to alternative loading

264 Figure 8 presents the experimental results of saturated sand subjected to alternative axial strain
265 with $\varepsilon_a=\pm 0.40\%$ (CTT14-18) under distinct loading frequencies f from 0.01 to 5.00 Hz. The
266 stress-strain curves in Figure 8a show that the adopted PID controller functioned correctly as all
267 axial strains fell within the prescribed range in relation to the imposed loading despite the
268 significant increase in f . In terms of the deviator stress q , the amplitude value was much greater
269 on the compression side than that on the extension side. This asymmetrical property is in
270 accordance with the experimental observations reported in the literature [39]. The relationship
271 between Δu and N_{cyc} depicted in Figure 8b shows that (i) with the first minor increase in f (from
272 0.01 Hz in blue to 0.02 Hz in red), two curves almost coincide with each other and no clear
273 tendency upon f can be found; (ii) with the further huge increase (in particular to $f= 1.00$ and 5.00
274 Hz), the build-up of Δu remarkably decreased to be smaller with the increasing f . For strain-
275 controlled cyclic triaxial tests, r_u is commonly taken as a reasonable yardstick to identify the
276 onset of sand liquefaction [40], and a value of $r_u=0.90$ was thought in the present work. It can be
277 seen from Figure 8b that N_{cyc} required to the attainment of this considered criteria increased with
278 the increasing f , which is consistent with the observations in stress-controlled tests that the higher
279 loading frequency could suppress the progress of sand liquefaction.

280

281

282 4. Discussion

283 For granular materials such as sandy soil, the overall soil resistance to deformation (e.g., axial
284 stain in a cyclic triaxial test) beyond the elastic range is mainly the result of the irreversible
285 sliding of the sand grains against one another, which leads to the generation of the occlusal
286 friction represented by the reciprocal constraint of the adjacent sand grains on their relative
287 movements. From a microscopic viewpoint, this occlusal friction (in Figure 9) between the sand
288 grains could be determined considering the following two factors according to the friction law
289 ($f=N\times\mu$): (i) the normal force N perpendicular to the contact point standing for the compaction
290 degree of the sand grains, which can be globally represented by the effective confining pressure
291 σ'_c acting on the test specimen; and (ii) the fractional coefficient, μ , which can be represented by
292 the intrinsic frictional angle of the sand used. Thus, it can be logically deduced that (i) for sand
293 specimens composed of a given sand under a certain level of σ'_c , the occlusal friction against
294 external loading can be assumed to be constant as long as relative sliding occurs; (ii) **this**
295 **occlusal friction** is further irrespective of how fast [41,42] the relative sliding is. In the published
296 literature, the experimental investigations conducted by Semblat [43] and Song [44] indicated an
297 insignificant strain-rate effects on dry sand with stress magnitudes going up to 200 MPa and
298 strain rates in excess of 10000/s [45]. This reason could explain why very similar responses were
299 observed in the case of dry sand (e.g., CTT1-3), as shown in Figure 3.

300 The completely opposite phenomena (e.g., deformation range, effect of loading frequency)
301 pertaining to dry (e.g., CTT1-3) and saturated sand specimens (e.g., CTT4-7 and CTT14-18)
302 could be ascribed only to the saturation-dependency since all the other controlled parameters
303 were exactly identical. In the alternative loading pattern, the imposed loading (σ_a in stress-
304 controlled mode **and** ε_a in strain-controlled mode) could, in general, be divided into two different
305 parts: (i) extension half cycles with $q<0$ and (ii) compression half cycles with $q>0$. In the former
306 case, the test specimen was stretched due to the reduction in the **deviator** stress, owing to which,
307 the test specimen exhibited a macroscopic necking form. In this process, for the saturated
308 specimen, the sand grains slid away from one another. Consequently, the corresponding Δu was
309 **globally** adjusted to be negative (as justified in Figure 5b) so as to maintain the total specimen
310 volume as constant. In the latter case, the test specimen was compressed due to the increase in
311 the **deviator** stress, owing to which, the test specimen exhibited a macroscopic barrel form. In

312 contrast to the extension cycles, the sand grains slid to approach one another, and the
313 corresponding Δu was adjusted to be positive (as proved in Figure 6b) so as to offset the volume-
314 contraction tendency. With regard to this fully saturated state, it should be considered that (i)
315 certain parts of the sand grains were likely suspended in the pore water and lost intergranular
316 contacts owing to the positive Δu , which facilitated the further generation of ε_a in the consequent
317 extension cycles; and (ii) the large degree of ε_a generated in the extension cycles promoted the
318 further rapid build-up of Δu in the consequent compression cycles. Under the abovementioned
319 reciprocal effects pertaining to the **alternative cycles (compression with extension)**, an
320 increasingly enhanced softening liquefaction response may be expected. This aspect could
321 explain why under the same experimental conditions, the strain range of the saturated sand
322 specimens **in stress-controlled tests** was obviously more important than that of the dry sand
323 specimens. However, this argument could not legitimately elucidate the effect of the loading
324 frequency on the response of the saturated sand specimens (as shown in Figure 4) because the
325 sliding between the sand grains is still independent of the loading speed even under large ε_a . As
326 the time interval at which deformation occurs becomes very short in cyclic triaxial tests, it is to
327 be borne in the mind that inertia force **of sand grains themselves** is another kind of agency that
328 needs to be critically taken into account in the range of the transient deformation associated with
329 sand liquefaction. In general, the inertia force that characterizes the dynamic behaviour as
330 distinguished from the static one [33,45–47] depends on the (i) mass of the sand grains and (ii)
331 acceleration linked to the strain rate of the considered sand grains. Figure 10 schematizes a
332 conceptual model of the inertia force appearing in extension and compression half cycles,
333 respectively. In the axial direction, in the case of the extension cycles depicted in Figure 10a, the
334 inertia force appears opposite to the sand grains' movement, thereby enhancing the resistance to
335 the applied axial loading. In the case of the compression cycles, as shown in Figure 10b, the
336 presence of inertia force equally makes a beneficial contribution to the axial resistance in the
337 same manner. In other words, when the strain rate of the test specimen becomes conspicuously
338 important (e.g., in the case of transient deformation while approaching or attaining the
339 liquefaction response), the test specimen cannot experience a sufficient time lag, allowing the
340 full build-up of **sand liquefaction** to be achieved since the applied loading rapidly reverses its
341 direction in the cases of higher loading frequencies. This mechanism is capable to inhibit the
342 accumulated development of ε_a [48] **in stress-controlled tests and Δu in strain-controlled tests**. It

343 explains why a remarkable effect of the loading frequency occurred in saturated sand specimens
344 subjected to alternative loading. In this sense, a similar phenomenon should also be observed in
345 the case of dry sand specimens. However, the experimental results derived from Figure 3a do not
346 support this argument. This phenomenon might be attributed to the fact that without the presence
347 of Δu in the dry state, the deformation of dry sand grains can be considered as being quasi-static,
348 resulting in an ignorable effect of loading frequency.

349 For the lateral direction in the extension (see Figure 10a) and compression (see Figure
350 10b) cycles, two distinct mechanisms can be identified: the inertia force (i) exists in the form of
351 weakening the lateral confinement on the extension side and (ii) still makes a positive
352 contribution to the lateral confinement on the compression side. As explained in the foregoing
353 section, the relative sliding between the adjacent sand grains, yielding global resistance, is
354 proportional to the normal force N , as represented by the confinement level. Hence, the presence
355 of lateral inertia force in the compressive/extension cycles enhances and weakens the specimen
356 resistance to deformation, respectively. In addition, when the sand specimens are deposited
357 under gravity, it has been experimentally demonstrated [49,50] that the long axes of the sand
358 grains preferentially orient along the horizontal direction so as to achieve a naturally stable state.
359 Under pure compressive loading, the rearrangement of the sand grains occurs in a more stable
360 horizontal direction (e.g., barrel effect), whilst a totally reversed phenomenon could then be
361 expected for pure extensional loading (e.g., necking effect). By combining the above two factors,
362 it can be deduced that under the same level of loading (e.g, T_{cc}) with opposite loading directions
363 (compression versus extension), the resistance to deformation should be much more prevailing in
364 compressive loading than in extensional loading. This aspect could explain why a greater strain
365 range and transient deformation only occurred for test specimens subjected to non-alternative
366 extensional loading, during which the effect of loading frequency (experimentally justified by
367 Figure 5 and Figure 7) should necessarily be considered with the inertia force, as explained
368 previously. On the contrary, due to the lack of the above two key factors (considerably strain
369 range and transient deformation), the effect of the loading frequency ($f=0.02-0.30$ Hz employed
370 in the present work) could be logically assumed to be of second importance in the case of non-
371 alternative compressive loading, which is highly consistent with the experimental results
372 displayed in Figure 6 and Figure 7.

373 5. Conclusions

374 In this study, the effect of the loading frequency f was investigated by performing (i) stress-
375 controlled cyclic triaxial tests for dry and saturated sand specimens in the dense ($I_{Dmat}=0.70$) and
376 medium-dense ($I_{Dmat}=0.55$) states subjected to alternative and non-alternative loadings; and (ii)
377 strain-controlled cyclic triaxial tests for saturated dense sand specimens ($I_{Dmat}=0.70$) over a wide
378 range of f . The results can be used to derive the following conclusions:

- 379 1) Under alternative loading, dry sand specimens with $I_{Dmat}=0.70$ (CTT1-3) deformed
380 almost in a quasi-static manner and were insensitive to the variation in f , which
381 eliminated the need to consider the additional inertia force.
- 382 2) In the presence of pore water, the saturated sand specimens with $I_{Dmat}=0.70$ subjected to
383 alternative loading indeed liquefied with transient deformation. In stress-controlled mode
384 (CTT4-7), the effect of the f was required to be carefully considered, especially after the
385 triggering of transient deformation associated with sand liquefaction. In strain-controlled
386 mode (CTT14-18), a significant effect of f was also found when the applied f was
387 drastically increased. In these two cases, the presence of inertia force opposing the
388 applied loading in the axial direction is the main reason to explain the above experimental
389 observations.
- 390 3) In the case of non-alternative loading in pure extensional loading for stress-controlled
391 tests, a higher f also made a beneficial contribution to axial resistance for medium-dense
392 saturated sand specimens with $I_{Dmat}=0.55$ owing to the presence of the axial inertia force,
393 very similar to the alternative loading for saturated specimens in dense state ($I_{Dmat}=0.70$).
394 In contrast, no clear effect of f was observed in the case of pure compressive loading,
395 which could be ascribed to the following two factors: (i) the inertia force in the lateral
396 direction appeared in the form of enhancing lateral confinement, thereby impeding the
397 relative sliding; and (ii) during shearing, the rearrangement of the sand grains took place
398 in a more stable direction. Therefore, the sand specimens only deformed in a moderate
399 manner without transient defamation leading to an ignorable effect of the f .

400

401 Acknowledgements

402 The authors acknowledge the support of the geotechnical laboratory of Ecole des Ponts
403 ParisTech. The financial support provided by the research sponsors through ANR ISOLATE and
404 the inspiring discussion on dynamic issues with Dr. Li are deeply acknowledged.

405

406 Reference

- 407 [1] Ishihara K, Koga Y. Case Studies of Liquefaction In the 1964 Niigata Earthquake. *Soils*
408 *Found* 1981;21:35–52.
- 409 [2] Wyss M, Brune J. The Alaska earthquake of 28 March 1964: A complex multiple rupture.
410 *Bull Seismol Soc Am* 1967;57:1017–23.
- 411 [3] Ni X, Ye B, Ye G, Zhang F. Unique determination of cyclic instability state in flow
412 liquefaction of sand. *Mar Georesources Geotechnol* 2020;0:1–9.
413 <https://doi.org/10.1080/1064119X.2020.1791289>.
- 414 [4] Seed H, Idriss I, Makdisi F, Banerjee N. Representation of irregular stress time histories
415 by equivalent uniform stress series in liquefaction analyses. Berkeley: 1975.
- 416 [5] Benghalia Y, Bouafia A, Canou J. Comportement mécanique des sols sableux avec un
417 indice des vides intergranulaire constant. 8ème Colloq. Natl. afps, 2011.
- 418 [6] Benahmed N. Comportement mécanique d'un sable sous cisaillement monotone et
419 cyclique: application aux phénomènes de liquéfaction et de mobilité cyclique. Ph.D Thesis
420 Ecole Nationale Des Ponts et Chaussées, 2001.
- 421 [7] Jradi L. Study of the Influence of Fine Particles on the Properties of Liquefaction of Sands.
422 Ph.D Thesis University Paris-Est, 2018.
- 423 [8] Suzuki M, Yamamoto T. Liquefaction Characteristic of Undisturbed Volcanic in Cyclic
424 Triaxial Test. 13th World Conf. Earthq. Eng. Vancouver, 2004.
- 425 [9] Ghionna VN, Porcino D. Liquefaction resistance of undisturbed and reconstituted samples
426 of a natural coarse sand from undrained cyclic triaxial test. *J Geotech Geoenvironmental*
427 *Eng* 2006;132:194–202. [https://doi.org/10.1061/\(ASCE\)1090-0241\(2006\)132](https://doi.org/10.1061/(ASCE)1090-0241(2006)132).
- 428 [10] Sitharam TG, GovindaRaju L, Srinivasa Murthy BR. Evaluation of liquefaction potential
429 and dynamic properties of silty sand using cyclic triaxial testing. *Geotech Test J*
430 2004;27:423–9. <https://doi.org/10.1520/gtj11894>.
- 431 [11] Saxena SK, Reddy KR, Avramidis AS. Liquefaction resistance of artificially cemented
432 sand. *J Geotech Eng* 1988;114:1395–413.

- 433 [12] Silva WJ. Soil response to earthquake ground motion. 1988.
- 434 [13] Kramer SL. Geotechnical Earthquake Engineering. 1996.
- 435 [14] Boore DM, Bommer JJ. Processing of strong-motion accelerograms: Needs, options and
436 consequences. *Soil Dyn Earthq Eng* 2005;25:93–115.
437 <https://doi.org/10.1016/j.soildyn.2004.10.007>.
- 438 [15] Ye B, Xie X, Zhao T, Song S, Ma Z, Feng X, et al. Centrifuge Tests of Macroscopic and
439 Mesoscopic Investigation into Effects of Seismic Histories on Sand Liquefaction
440 Resistance. *J Earthq Eng* 2020;00:1–23. <https://doi.org/10.1080/13632469.2020.1826373>.
- 441 [16] Peacock WH, Seed HB. Sand liquefaction under cyclic loading simple shear conditions. *J*
442 *Soil Mech Found Div* 1968:689–708.
- 443 [17] YOSHIMI Y, OH-OKA H. Influence of Degree of Shear Stress Reversal on the
444 Liquefaction Potential of Saturated Sand. *Soils Found* 1975;15:27–40.
- 445 [18] Tatsuoka F, Maeda S, Fujii S, Yamada S. Cyclic Undrained Strengths of Saturated Sand
446 under Random and Uniform Loading and Their Relation 1983.
- 447 [19] Tatsuoka F, Toki S, Miura S, Kato H, Okamoto M, Yamada S, et al. Some factors
448 affecting cyclic undrained triaxial strength of sand. *Soils Found* 1986;26:96–116.
- 449 [20] Polito CP. The Effects Of Non-Plastic and Plastic Fines On The Liquefaction Of Sandy
450 Soils. Virginia Polytechnic Institute and State University, 1999.
- 451 [21] Nong Z, Park S, Jeong S-W, Lee D-E. Effect of Cyclic Loading Frequency on
452 Liquefaction Prediction of Sand. *Appl Sci* 2020;10:4502.
- 453 [22] Lee KL, Fitton JA. FACTORS AFFECTING THE CYCLIC LOADING STRENGTH OF
454 SOIL. *Vib Eff Earthquakes Soils Found* 1969:71–95. <https://doi.org/10.1520/STP33637S>.
- 455 [23] Guo Y, He L. The Influences of the Vibration Frequencies on Liquefaction Strength of
456 Saturated Sands. *J Disaster Prev Mitig Eng* 2009;29:618–22.
457 <https://doi.org/10.13409/j.cnki.jdpme.2009.06.015>.
- 458 [24] Feng T, Zhang L. Experimental study on effect of vibration frequency on dynamic
459 behaviors of saturatd sands. *J Water Resour Archit Eng* 2013;11:11-14,76.

- 460 [25] ZHANG S, ZHANG Y, ZHANG L, LIU C. Influence of Confining Pressure and Vibration
461 Frequency on the Liquefaction Strength of the Saturated Gravel Sand. *J Xinjiang Agric*
462 *Univ* 2015;38:68–71.
- 463 [26] Zhang J, Cao J, Huang S. Experimental Study on the Effects of Initial Shear Stress and
464 Vibration Frequency on Dynamic Strength of Saturated Sands. *Adv Mater Sci Eng*
465 2019;2019:1–9. <https://doi.org/10.1155/2019/3758527>.
- 466 [27] Mulilis JP, Chan, C K, Seed HB. The effects of method of sample preparation on the
467 cyclic stress-strain behavior of sands (EERC Report 75-18). University of California:
468 Berkeley, CA, USA: 1975.
- 469 [28] Dash HK, Sithara TG. Effect of frequency of cyclic loading on liquefaction and dynamic
470 preoperties of saturaed sand. *Int J Geotech Eng* 2016;10:487–92.
- 471 [29] Zhu Z, Dupla J, Canou J, Foerster E. Experimental study of liquefaction resistance : effect
472 of non-plastic silt content on sand matrix. *Eur J Environ Civ Eng* 2020;0:1–19.
473 <https://doi.org/10.1080/19648189.2020.1765198>.
- 474 [30] Yang J, Wei LM. Collapse of loose sand with the addition of fines: The role of particle
475 shape. *Geotechnique* 2012;62:1111–25. <https://doi.org/10.1680/geot.11.P.062>.
- 476 [31] Zhu Z, Zhang F, Peng Q, Chabot B, Dupla J. Development of an auto compensation
477 system in cyclic triaxial apparatus for liquefaction analysis. *Soil Dyn Earthq Eng*
478 2021;144:106707. <https://doi.org/10.1016/j.soildyn.2021.106707>.
- 479 [32] Zhu Z, Kham M, Fernandes VA, Lopez-Caballero F. Dynamic Response of a Central Clay
480 Core Dam Under Two-Component Seismic Loading. *Springer Ser Geomech Geoengin*
481 2020;1:231–6. https://doi.org/10.1007/978-3-030-46351-9_23.
- 482 [33] Ishihara K. *Soil Behaviour in Earthquake Geotechnics*. Oxford science publications; 1995.
- 483 [34] Zhu Z, Zhang F, Dupla JC, Canou J, Foerster E. Investigation on the undrained shear
484 strength of loose sand with added materials at various mean diameter ratios. *Soil Dyn*
485 *Earthq Eng* 2020;137. <https://doi.org/10.1016/j.soildyn.2020.106276>.

- 486 [35] Yoshimi Y, Tokimatsu K, Kaneko O, Makihara Y. Undrained Cyclic Shear Strength of a
487 Dense Niigata Sand. *Soils Found* 1984;24:131–45.
488 https://doi.org/10.3208/sandf1972.24.4_131.
- 489 [36] Evans M, Zhou S. Cyclic behavior of gravelly soil. *Gr Fail Under Seism Cond ASCE*
490 1994:158–76.
- 491 [37] Li G. *Advanced Soil Mechanics*. TsingHua University; 2004.
- 492 [38] Li G, Guo RP. Volume contraction in unloading of shear tests and reversible dilatation of
493 soils. *Chinese J Geotech Eng* 2000;02:158–61.
- 494 [39] Kumar SS, Krishna AM, Dey A. Evaluation of dynamic properties of sandy soil at high
495 cyclic strains. *Soil Dyn Earthq Eng* 2017;99:157–67.
496 <https://doi.org/10.1016/j.soildyn.2017.05.016>.
- 497 [40] HAZIRBABA K, RATHJE E. A comparison between in situ and laboratory
498 measurements of pore water pressure generation. 13th Wo, Vancouver: 2004, p. 1220.
- 499 [41] Xie DY. *Soil dynamics*. Beijing: Higher Education Press; 2011.
- 500 [42] Horn HM, Deere DU. Frictional characteristics of minerals. *Geotechnique* 1962;12:319–
501 35.
- 502 [43] Semblat JF, Phong LM, Gray G. 3D-Hopkinson Bar: New Experiments for Dynamic
503 Testing on Soils. *Soils Found* 1999;39:1–10.
- 504 [44] Song B, Chen W, Luk V. Impact compressive response of dry sand. *Mech Mater*
505 2009;41:777–85. <https://doi.org/10.1016/j.mechmat.2009.01.003>.
- 506 [45] Omidvar M, Iskander M, Bless S. Stress-strain behavior of sand at high strain rates. *Int J*
507 *Impact Eng* 2012;49:192–213. <https://doi.org/10.1016/j.ijimpeng.2012.03.004>.
- 508 [46] Whitman RV, Healy KA. Shear strength of sands during rapid loadings. *J Soil Mech*
509 *Founadations Div ASCE* 1962;88(SM2):99–132.
- 510 [47] Whitman R V. *The response of soils to dynamic loadings*. 1970.

- 511 [48] Aghaei Araei A, Reza Razeghi H, Hashemi Tabatabaei S, Ghalandarzadeh A. Loading
512 frequency effect on stiffness, damping and cyclic strength of modeled rockfill materials.
513 Soil Dyn Earthq Eng 2012;33:1–18. <https://doi.org/10.1016/j.soildyn.2011.05.009>.
- 514 [49] Oda M. Initial fabric and their relations to mechanical properties of granular material. Soils
515 Found 1972;12:17–36.
- 516 [50] Yang ZX, Li XS, Yang J. Quantifying and modelling fabric anisotropy of granular soils.
517 Geotechnique 2008;58:237–48. <https://doi.org/10.1680/geot.2008.58.4.237>.
- 518

Table 1 Summary of the literature review pertaining to the loading frequency effect

No	Reference	Sand	Test Method	σ'_c (kPa)	I_d	Failure criteria	f (Hz)	Frequency Effect
1	Peacock [16]	Monterey	SST ⁽¹⁾	500	0.50	$r_u=1$	0.17-4	
2	Yoshimi [17]	Bandaijima	RTT ⁽²⁾	95.2	≈ 0.40	$r_u=1$	1-12	
3	Tatsuoka [18]	Toyoura	CTT ⁽³⁾	98	0.50-0.80	$\varepsilon_a=10\%$ (DA ⁽⁴⁾)	0.05, 0.50	minor
4	Tatsuoka [19]	Toyoura	CTT	100	0.50	$\varepsilon_a=10\%$ (DA)	0.05-1	
5	Polito [20]	Monterey	CTT	100	0.74	$r_u=1$	0.50, 1	
6	Lee [22]	EI Monte and Silt	CTT	103	0.50, 0.75	$\varepsilon_a=5\%, 10\%$ or 20% (DA)	0.17-1	
7	Guo [23]	NA ⁽⁴⁾	CTT	100-300	0.28, 0.70	$r_u=1$	0.05-1	
8	Feng [24]	Fujian sand	CTT	50	0.30	$r_u=1$	0.05-2	stable at higher f
9	Zhang [25]	NA	CTT	100	0.65	$r_u=1$	0.50-2	
10	Zhang [26]	Wuchuan sand	CTT	50, 100, 150	0.55	$r_u=1$	1-3	
11	Nong [21]	Nakdong River sand	SST	50, 100, 200	0.40, 0.80	$\varepsilon_a=7.5\%$ (DA)	0.05-1	
12	Mulilis [27]	Monterey	CTT	100	0.50	$\varepsilon_a=5\%$ (DA)	0.017-1	
13	Dash [28]	Original Ahmadabad sand	CTT	100	0.54	$r_u=1$	0.10-0.50	stable at lower f

Note:(1) SST: simple shear test; (2) RTT: ring torsion test; (3) CTT: cyclic triaxial test; (4) DA: double amplitude
(5) NA: not available

521

Table 2 Physical properties of the test material

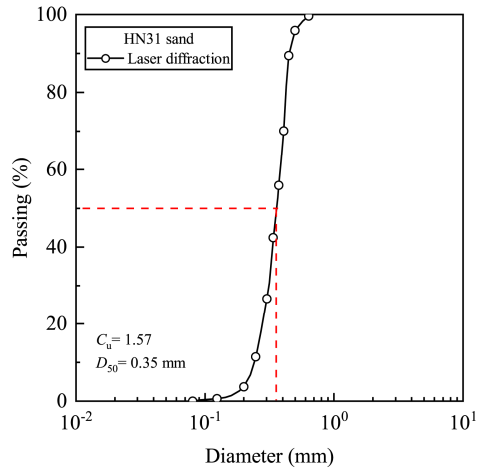
Material	D_{50} (μm)	C_u	e_{min}	e_{max}	G_s	I_p
HN31	350	1.57	0.656	1	2.65	Non-plastic

522

Table 3 Cyclic triaxial test programme

Reference	$I_{Dmat}^{(1)}$		Loading Pattern	S_r (%) ⁽⁶⁾	f (Hz)	Control mode	σ'_c (kPa)	Waveform
		$T_{cc}^{(2)}$						
CTT1					0.02			
CTT2	0.70	0.22	A ⁽³⁾	0	0.10			
CTT3					0.60			
CTT4					0.02			
CTT5	0.70	0.22	A		0.10	Stress		
CTT6					0.30			
CTT7					0.60			
CTT8					0.02			
CTT9	0.55	0.60	NA(E) ⁽⁴⁾	100	0.10			
CTT10					0.60		100	Sine
CTT11					0.02			
CTT12	0.55	0.60	NA(C) ⁽⁵⁾		0.10			
CTT13					0.60			
		ϵ_a						
CTT14					0.01			
CTT15					0.02	Strain		
CTT16	0.70	$\pm 0.40\%$	A	100	0.10			
CTT17					1.00			
CTT18					5.00			

Note:(1) Density index of sand matrix: I_{Dmat} ; (2) Cyclic stress ratio: T_{cc}
(3) Alternative loading: A; (4) Non-Alternative extensional loading: NA(E)
(5) Non-Alternative compressive loading: NA(C); (6) Saturation degree: S_r

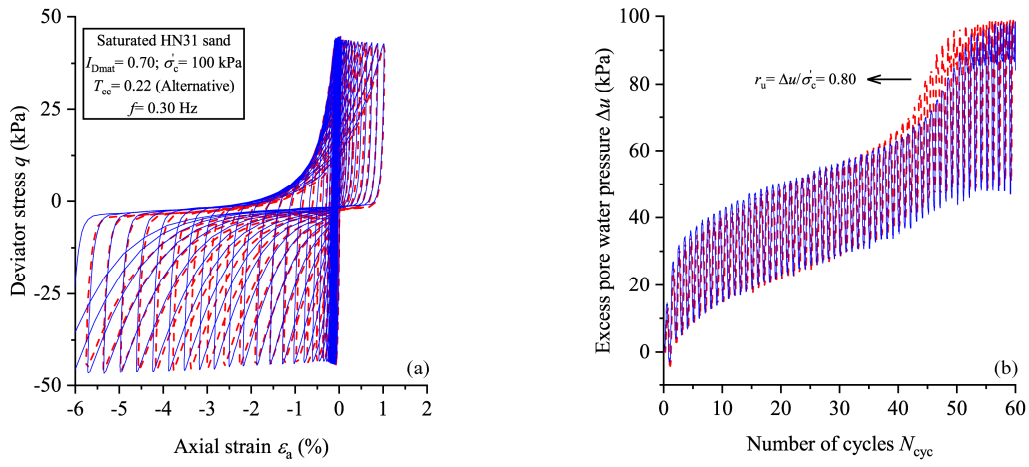


527

528

Figure 1 Grain size distribution curve of HN31 sand.

529



530

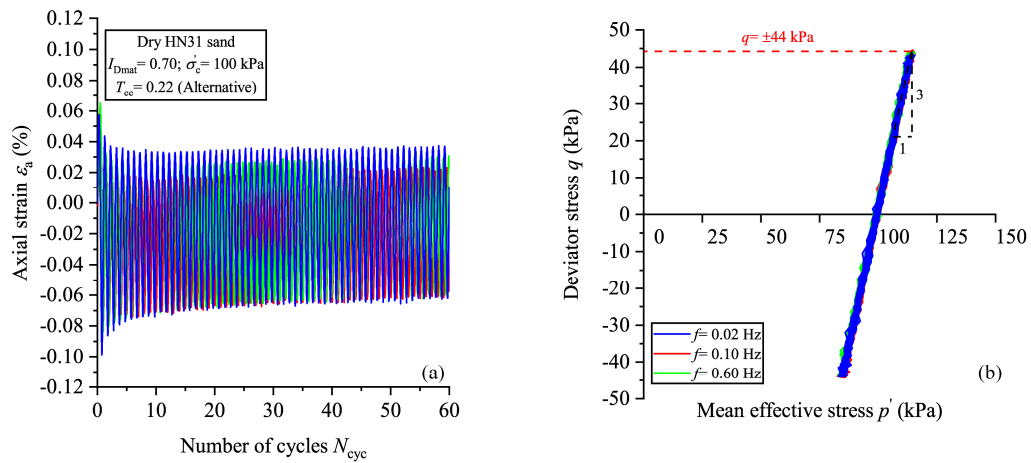
531

532

533

534

Figure 2 Repeatability tests of specimens CTT6 with $I_{Dmat}=0.70$, $\sigma'_c=100$ kPa, $T_{cc}=0.22$ (Alternative) and $f=0.30$ Hz in terms of (a) stress-strain; and (b) excess pore water pressure-number of cycles curves.



535

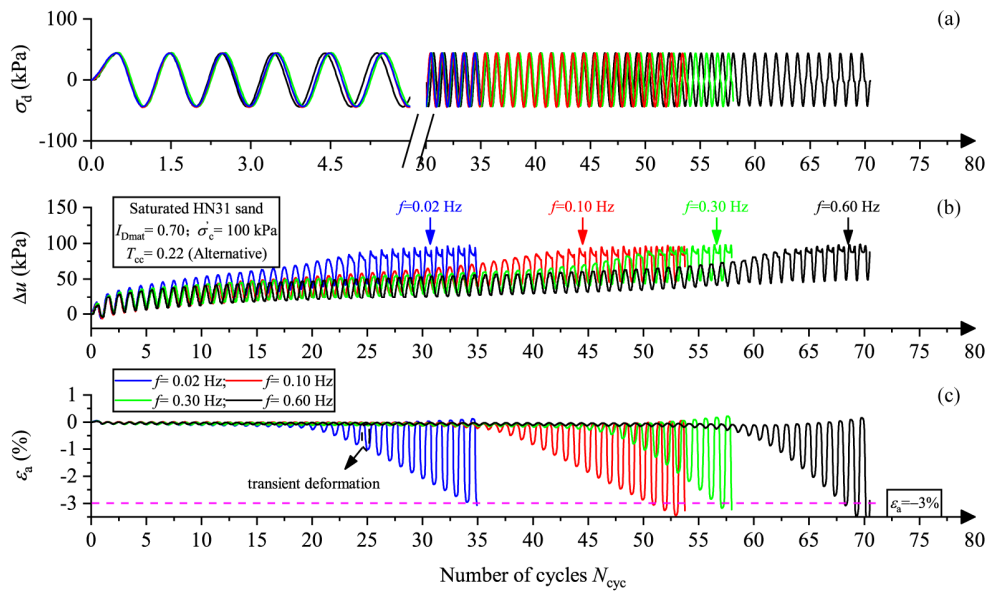
536 *Figure 3 Experimental results of dry sand specimens ($I_{Dmat}=0.70$, $\sigma'_c=100$ kPa) subjected to*
 537 *alternative shearing ($T_{cc}=0.22$) under distinct loading frequencies ($f=0.02$, 0.10 and 0.60 Hz) in*
 538 *terms of the (a) stress-number of cycles; and (b) effective stress paths curves.*

539

540 **This figure is requested to be printed in color.**

541

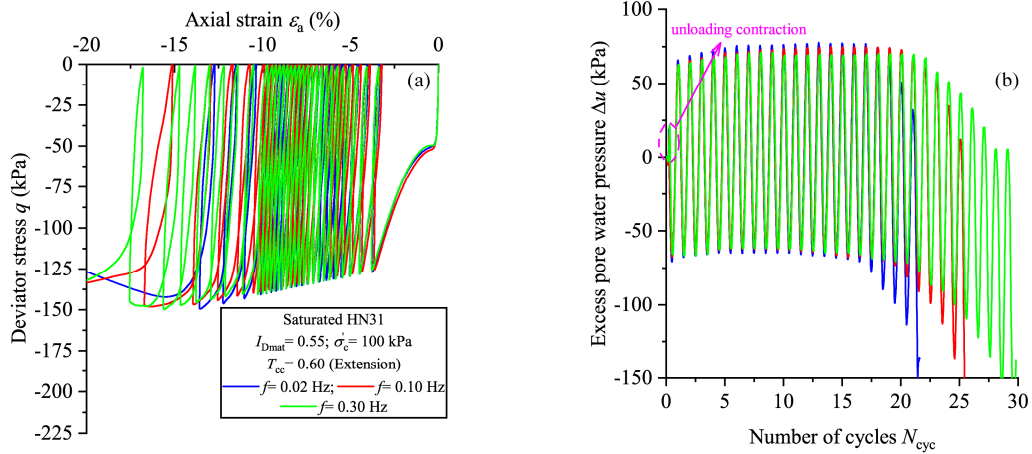
542



543

544 *Figure 4 Experimental results of saturated sand specimens ($I_{Dmat}=0.70$, $\sigma'_c=100$ kPa) subjected*
 545 *to alternative shearing ($T_{cc}=0.22$) under distinct loading frequencies ($f=0.02$, 0.10, 0.30 and*
 546 *0.60 Hz) in terms of the (a) deviator stress-; (b) excess pore water pressure-; and (c) axial*
 547 *strain-number of cycles curves.*

548



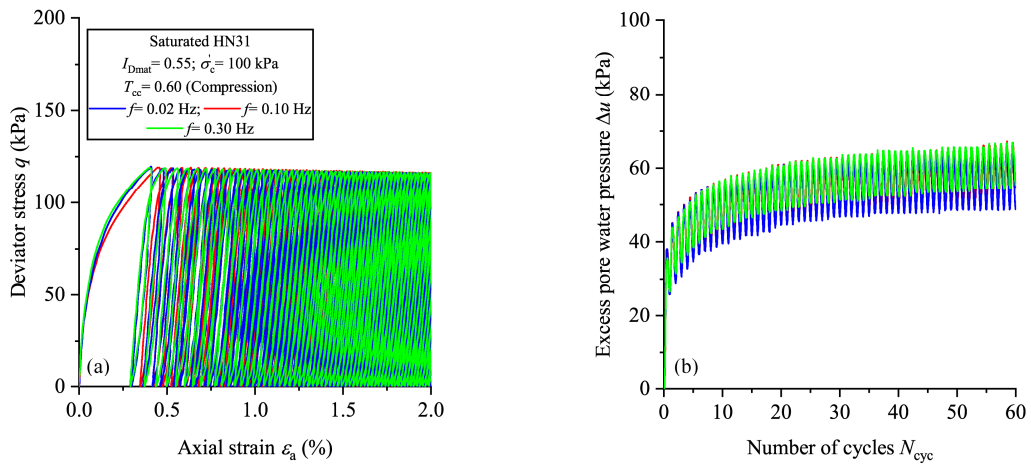
549

550 *Figure 5 Experimental results of saturated sand specimens ($I_{Dmat}=0.55$, $\sigma'_c=100$ kPa) subjected*
 551 *to non-alternative extensional shearing ($T_{cc}=0.60$) under distinct loading frequencies ($f=0.02$,*
 552 *0.10 and 0.60 Hz) in terms of the (a) stress-strain; (b) excess pore water pressure-number of*
 553 *cycles curves.*

554

555 **This figure is requested to be printed in color.**

556



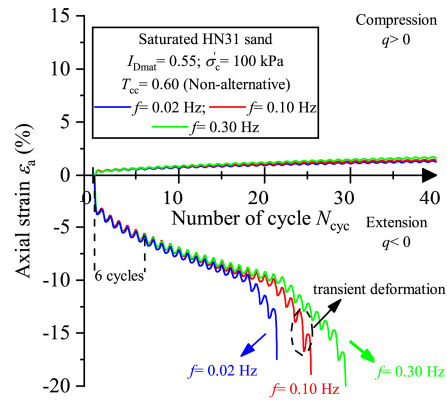
557

558 *Figure 6 Experimental results of saturated sand specimens ($I_{Dmat}=0.55$, $\sigma'_c=100$ kPa, $T_{cc}=0.60$)*
 559 *subjected to non-alternative compressive shearing ($T_{cc}=0.60$) under distinct loading frequencies*
 560 *($f=0.02$, 0.10 and 0.60 Hz) in terms of the (a) stress-strain; (b) excess pore water pressure-*
 561 *number of cycles curves.*

562

563 **This figure is requested to be printed in color.**

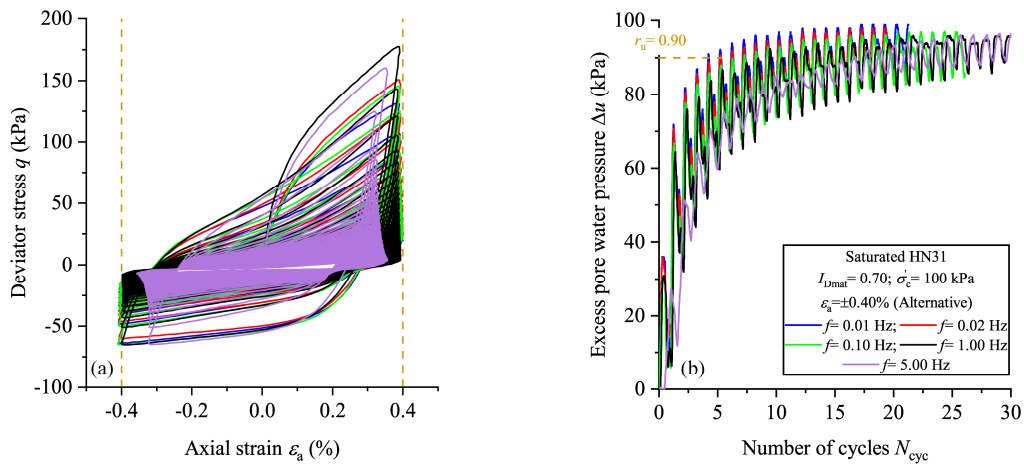
564



565

566 *Figure 7 Accumulated axial deformation developed in the non-alternative loading of saturated*
 567 *sand specimens ($I_{Dmat}=0.55$, $\sigma'_c=100$ kPa, $T_{cc}=0.60$) on the (a) compression; and (b) extension*
 568 *sides.*

569



570

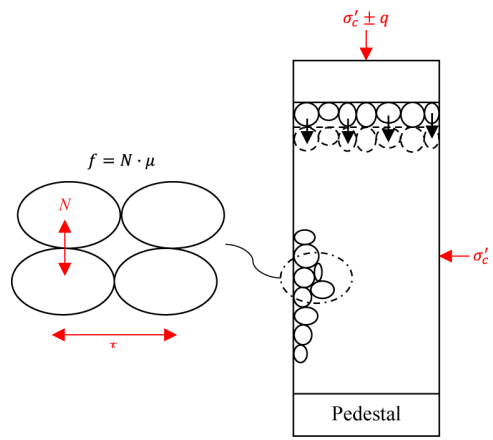
571 *Figure 8 Experimental results of saturated sand specimens ($I_{Dmat}=0.70$, $\sigma'_c=100$ kPa) subjected*
 572 *to alternative axial strain ($\varepsilon_a=\pm 0.40\%$) under distinct loading frequencies ($f=0.01$, 0.02, 0.10,*
 573 *1.00 and 5.00 Hz) in terms of the (a) stress-strain; and (b) excess pore water pressure-number of*
 574 *cycles curves.*

575

576 **This figure is requested to be printed in color.**

577

578



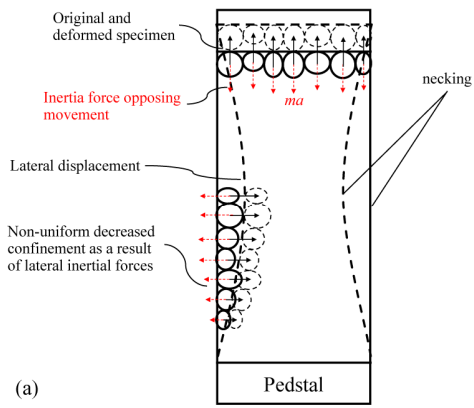
579

580

Figure 9 Schematic of occlusal friction of the dry sand specimen.

581

582



583

584

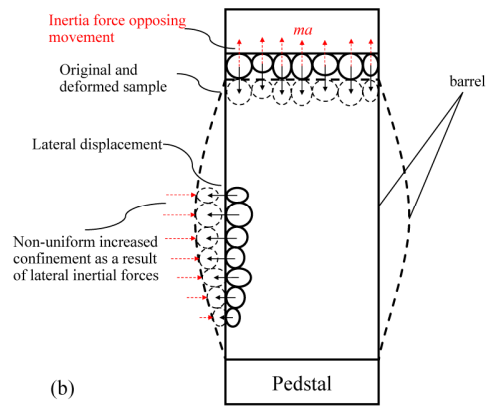


Figure 10 Schematic of the inertia force in the (a) extension and (b) compression cycles (modified from Omidvar [45]).